International Journal of Nanomedicine

Dovepress

open access to scientific and medical research

Open Access Full Text Article

ORIGINAL RESEARCH

Cetuximab-Modified Human Serum Albumin Nanoparticles Co-Loaded with Doxorubicin and MDR1 siRNA for the Treatment of Drug-Resistant Breast Tumors

Xin Yang[1–3]
Yifan Wang[1–3]
Si Chen[1–3]
Shuang Zhang[1–3]
Chunying Cui[1–3]

[1]School of Pharmaceutical Sciences, Capital Medical University, Beijing, 100069, People's Republic of China; [2]Engineering Research Center of Endogenous Prophylactic of Ministry of Education of China, Beijing, 100069, People's Republic of China; [3]Beijing Area Major Laboratory of Peptide and Small Molecular Drugs, Beijing, 100069, People's Republic of China

Correspondence: Chunying Cui; Shuang Zhang
Department of Pharmaceutics, School of Pharmaceutical Science, Capital Medical University, No. 10 Youanmenwai Street, Fengtai, Beijing, 100069, People's Republic of China
Tel/Fax +86-10-8391-1668; +86-10-8391-1673
Email ccy@ccmu.edu.cn; zshuang@ccmu.edu.cn

Background: Breast cancer is the most prevalent cancer among women. Doxorubicin (DOX) is a common chemotherapeutic drug used to treat many different cancers. However, multidrug resistance limits the treatment of breast cancer. MDR1 siRNA (siMDR1) combinatorial therapy has attracted significant attention as a breakthrough therapy for multidrug resistance in tumors. However, naked siRNA is easily degraded by enzymatic hydrolysis requiring an siRNA carrier for its protection. Human serum albumin (HSA) was selected as the carrier due to its excellent biocompatibility, non-toxicity, and non-immunogenicity. Cetuximab was used to modify the HSA nanoparticles in order to target the tumor tissues.

Methods: This study used a central composite design response surface methodology (CCD-RSM) to investigate the optimal formula for HSA NPs preparation. Cex-HSA/DOX/MDR1 siRNA (C-H/D/M) was characterized by dynamic light scattering and transmission electron microscopy. The efficacy of C-H/D/M tumor growth inhibitory activity was investigated in vitro and in vivo using confocal imaging, MTT assay, and an MCF-7/ADR tumor-bearing mice model. RT–qPCR, ELISA analysis, and flow cytometry were used to investigate the in vitro antitumor mechanisms of C-H/D/M.

Results: The diameter and PDI of the C-H/D/M were 173.57 ± 1.30 nm and 0.027 ± 0.004, respectively. C-H/D/M promoted and maintained the sustained release and the uptake of DOX significantly. After transfection, the MDR1 mRNA and P-gp expression levels were down-regulated by 44.31 ± 3.6% ($P < 0.01$) and 38.08 ± 2.4% ($P < 0.01$) in an MCF-7/ADR cell line. The fluorescent images of the treated BALB/c nude mice revealed that C-H/D/M achieved targeted delivery of siMDR1 and DOX into the tumor tissue. The in vivo tumor inhibition results demonstrated that the tumor inhibition rate of the C-H/D/M treated group was 54.05% ± 1.25%. The biosafety results indicated that C-H/D/M did not induce significant damages to the main organs in vivo.

Conclusion: C-H/D/M can be used as an ideal non-viral tumor-targeting vector to overcome MDR and enhance the antitumor effect.

Keywords: human serum albumin, HSA, multidrug resistance, MDR, co-delivery carrier, small interfere RNA, gene silencing

Introduction

Currently, the high incidence rates of tumors have increased significantly affecting, mortality and quality of life. Breast cancer is the most common cause of death and one of the most prevalent cancers among women worldwide.[1,2] As people pay more

Received: 6 August 2021
Accepted: 4 October 2021
Published: 16 October 2021

and more attention to cancer, the treatment strategies for tumors are gradually increasing, including surgery, chemotherapy, immunotherapy, and other methods. Studies have shown that phototherapeutic or chemotherapeutic nano-delivery systems can reduce metastasis through enhanced tumor-killing efficiency.[3,4] Doxorubicin is a commonly used chemotherapeutic drug within clinical practices and has an excellent anti-tumor effect against a variety of cancers, including breast cancer.[5] DOX breaks the DNA double strands and inhibits the actions of topoisomerase II, resulting in the apoptosis of cancer cells. However, the problem of drug resistance gradually emerging as the use of doxorubicin increases.[6,7] Tumor multidrug resistance (MDR) is a common phenomenon in various kinds of tumor cells. Tumor MDR's mechanism of action either lowers the intracellular concentration of the chemotherapeutic agent or makes the drug less efficacious; therefore, leading to the failure of the therapy.[8] Up until now, several mechanisms have been reported that contributes to the clinical MDR of cancers; however, many of the challenges of chemotherapeutic drug resistance have not been addressed.[9,10] Thus, there is an urgent need to develop effective therapeutic approaches and add them to anticancer drug therapies in order to treat clinical MDR. MDR is often associated with the over-expression of the drug efflux transporter P-glycoprotein (P-gp), which reduces the intracellular concentration of anticancer drugs.[11,12] P-gp is a 170 kDa plasma membrane glycoprotein encoded by the MDR-1 gene and belonging to the adenosine triphosphate (ATP)-binding cassette (ABC) superfamily is expressed at different levels in a variety of cell types.[13] Currently, researchers are looking for advanced therapies to inhibit P-gp mediated effusion activity.[14]

A large number of studies have been found to improve the efficiency of cancer treatment and reduce the multidrug resistance problem. Haggag et al studied the co-delivery of Ran-RCC1 inhibitory peptide (RAN-IP), and doxorubicin loaded into liposomal nanocarriers and delivered to breast cancer cells. Co-administration of RAN-IP was used to improve the sensitivity of DOX within breast cancer cell lines.[15] The use of RNA interference (RNAi) technology used to reverse multidrug resistance is a powerful treatment for reducing MDR gene expression.[16,17]

siMDR1 can be combined with protease to form the RNA-induced silencing complex (RISC). The double-stranded siRNA is incorporated into the RISC complex as a single strand in order to form an active RISC complex.[18,19] Then, RISC complementary binds to the target mRNA, inhibiting the expression of the MDR1 gene reducing the expression of the p-glycoprotein.[20–22] However, siRNA has numerous issues, such as a large molecular weight, negative charge surface charge, and serum instability. Therefore, it is necessary to develop a safe and effective delivery vector to deliver siRNA into the body; thus, producing the intended therapeutic effects at the site of the tumor.[23–26]

In cancer therapy, two commonly used drug delivery systems include viral and non-viral vectors. Viral vectors encompass retro and adenoviruses and have a high transfection efficiency; however, the biological safety issues such as cytotoxicity, high immunogenicity, and potential carcinogenicity limits their clinical application.[27] In addition, non-viral gene delivery vectors such as cationic lipids,[28] PLGA nanocapsules,[29–31] and lipid based nanoparticles[32] have become the focus within the field of drug delivery due to their biocompatibility and low systemic side effects. However, the transfection efficiency of non-viral vectors is not ideal in vivo. Therefore, it is necessary to search for a new non-viral vector delivery system with high efficiency and low toxicity.

Human serum albumin (HSA) nanoparticles have shown excellent efficacy and biocompatibility in the delivery of anti-tumor drugs.[33–35] HSA nanoparticles have the ability to target, load, and release chemotherapeutic drugs to the target tissues and cells. HSA NPs reduce the side effects of drugs and increase their efficacy when treating tumors.[36,37] There are currently few systems that utilize albumin for gene and drug co-delivery.

This study used an endogenous biological macromolecule (HSA NPs) due to their advantages of biodegradability, non-toxicity, and non-immunogenicity. The three-dimensional structure of HSA is heart-shaped and has three domains. Both domains I and III have a bag-like structure formed by hydrophobic and positively charged groups. The HSA-based carriers can achieve enhanced accumulation at the tumor site due to overexpressing serum albumin-binding proteins various tumors.[38] Moreover, HSA NPs can bind to the albumin receptor gp60 expressed on tumor tissues.[39]

Although albumin has targeting effects, its targeting specificity is minimal. Monoclonal antibodies specifically bind to tumor surface-related antigens and transfer drugs, genes, and other therapeutic compounds to tumor cells while having little impact on normal

tissues. In this study, cetuximab is used to modify the HSA nanoparticles.[40–42] The epidermal growth factor receptor (EGFR) is overly expressed on the surface of MCF-7/ADR cells. Cetuximab is targeted to EGFR; thus, it can be used to modify HSA nanoparticles and specifically target cells and tissue that overexpress the receptor.[43,44]

The study aims to design an optimized nanoparticle formulation with a small size by varying different physical factors. HSA NPs can be used to deliver DOX and siMDR1 simultaneously to the site of the tumor in order to enhance the gene silencing and cytotoxic activity. (Figure 1) After modifying the NP's with cetuximab, we evaluated the physicochemical characterizations, cell uptake, MDR1 silencing efficiency, cell migration and invasion, cellular proliferation, and apoptosis in an MCF-7/ADR cell line. Therefore, this study synthesizes a drug delivery platform for the co-delivery of DOX and siMDR1, offering a novel strategy to overcome drug resistance.

Materials and Methods

Materials, Cells and Animals

Materials

Human serum albumin, penicillin, streptomycin, Doxorubicin hydrochloride (DOX·HCl) and 3-(4,5-dimethylthiazol-2-yl)-2,5-diphenyltetrazolium bromide (MTT) were purchased from Sigma-Aldrich. Lipo™2000 was purchased from Thermo Fisher Scientific (Waltham, MA, USA). Human MDR1 ELISA kit, High-Capacity cDNA Reverse Transcription Kit, High Capacity RNA-to-cDNA Kit, and Trizol were obtained from Thermo Fisher Scientific. HyClone Laboratories Inc (Logan, UT, USA) provided Roswell Park Memorial Institute 1640(RPMI 1640), fetal bovine serum (FBS), and trypsin. Bicinchoninic acid (BCA) protein kit was purchased from Pierce (Rockford, IL, USA). Matrigel was obtained from BD Biosciences (San Jose, CA, USA). siMDR1 and Cy5-siMDR1 were purchased from Gene-Pharma Co, Ltd (Shanghai,

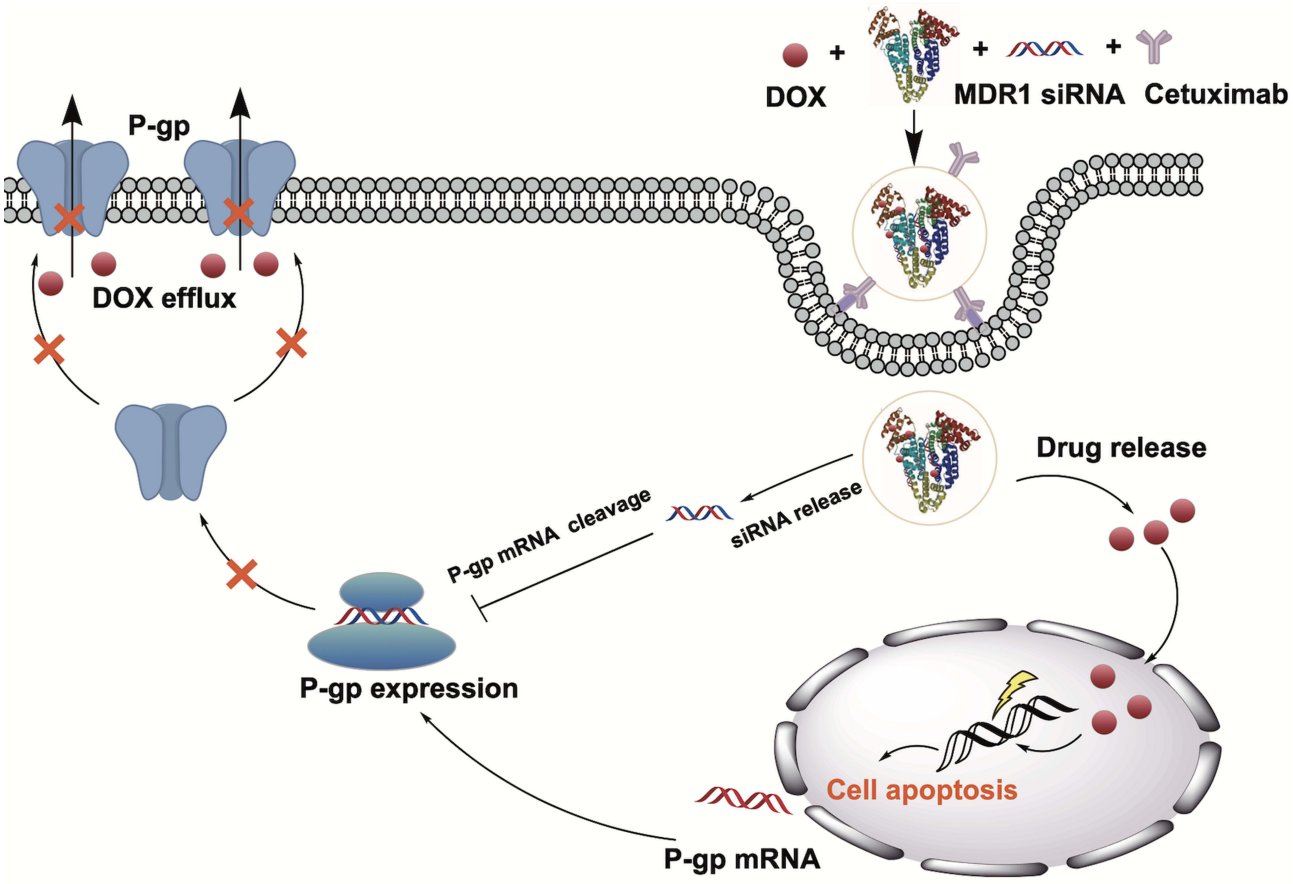

Figure 1 Schematic illustration of mechanisms and preparation of Cex-HSA/DOX/siMDR1. Cex-HSA/DOX/siMDR1 were prepared by the desolvation-crosslinking method, functionalization with cetuximab. After targeted into tumor tissues, Cex-HSA/DOX/siMDR1 could deliver DOX and siMDR1 into cells successfully, and DOX could be released to perform the antitumor effect.

China). Other chemicals and reagents were of analytical grade.

The sequences of siMDR1 are sense: 5′ GGAAAAGAAACCAACUGUCTT3′ and antisense: 5′ GACAGUUGGUUUCUUUUCCTT3′

Cells

MCF-7 human breast tumor cells and MCF-7/ADR human breast tumor cells were obtained from the Cancer Hospital of the Chinese Academy of Medical Sciences. MCF-7 cells and MCF-7/ADR cells were cultured in RPMI-1640 medium containing 1% penicillin and streptomycin, 10% FBS, and incubated at 37°C with 5% CO_2. The cells were subcultured 3 times a week until they reached 80% confluence.

Animals

Specific pathogen free (SPF) female BALB/c nude mice (4–6 weeks, 15–17 g) were purchased from the Animal Department of the Capital Medical University (Beijing Laboratory Animal Center, Beijing, China). The trial followed the Health Guidelines of the Capital Medical University and was approved by the Institutional Animal Ethics Committee of the Capital Medical University (The ethical code: AEEI-2019-132. Date of approval: 12th October 2019).

Prescription Optimization of HSA NPs

Human Serum Albumin Nanoparticles (HSA-NPs) were prepared using a desolvation-crosslinking method. In brief, HSA (1 mg) was carefully added to a NaCl (1 mL,10 mM) solution, and stirred for 15 minutes at room temperature (RT). Adjusting the pH value of the solution to 8.0, ethanol was added drop wise (1 mL/min) into the suspension. After stirring for 3 hours, 5 μL 8% glutaraldehyde aqueous solution was added to the suspension. Finally, the nanoparticle suspension was purified by centrifugation (12,000 rpm, 30 min, x3).

Six characteristics related to the preparation of the HSA NPs were investigated simultaneously (HSA concentration, pH value, volume of ethanol added, speed of ethanol addition, stirring rate, and glutaraldehyde concentration). The hydrodynamic diameter and polydispersity index (PDI) were used to evaluate the effects of the six characteristics.

Four factors that significantly influenced the diameter and PDI were selected. The central composite design (CCD) was employed to fit a polynomial model and obtain the optimal prescription.[45] Based on single factor experiments, four-parameter (HSA concentration (X1), pH value (X2), volume of ethanol (X3), and the speed of ethanol addition (X4)) were applied to optimize the diameter (Y1), PDI (Y2), and Zeta (Y3) using Design Expert 11 (trial version). 30 groups of experiments were designed. The response and the corresponding parameters were modeled and optimized using analysis of variance (ANOVA). According to the results, formula optimization was determined.

Preparation and Characterization of C-H/D/M NPs

DOX Loading

HSA and DOX were carefully added to a NaCl (1 mL,10 mM) solution, and stirred for 60 min at room temperature (RT). Then, the pH value of the solution was adjusted to 8.0; ethanol was added drop wise (1 mL/min) into the suspension. 5 μL of a 8% glutaraldehyde aqueous solution was added. The nanoparticle suspension was purified by centrifugation (12,000 rpm, 30 min, x3). The supernatant was collected and measured at a UV absorbance of 480 nm. The standard curve of the concentration versus absorbance was drawn to obtain the concentration of DOX.

siMDR1: Agarose Gel Retardation Assay

HSA and siRNA was carefully added to a NaCl (1 mL,10 mM) solution, and stirred for 15 minutes at room temperature (RT). Adjusting the pH value of the solution to 8.0, ethanol was added drop wise (1 mL/min) into the suspension. After stirring for 3 hours, 5 μL 8% glutaraldehyde aqueous solution was added to the suspension. Finally, the nanoparticle suspension was purified by centrifugation (12,000 rpm, 30 min, x3). The loading of siMDR1 into HSA NPs was analyzed quantitatively via an agarose gel retardation assay. HSA/DOX/siMDR1 (H/D/M) were prepared and evaluated at different w/w ratios (1:3, 1:2, 1:1, 1:0.9, 1:0.8, 1:0.5, and 1:0). The nanoparticles suspension was purified by centrifugation (12,000 rpm, 30 min, x3). The supernatant was collected and electrophoresed in 1% (w/v) agarose gel containing ethidium bromide (2 mg/mL) at a constant voltage of 120 V for 20 minutes. The results were imaged by a UV transilluminator.

Surface Modification of the H/D/M

For the antibody modification of the nanoparticles, activation of the particle surface was performed. 8.8 mg of the heterobifunctional PEG cross-linker NHS- PEG3500-Mal in 500 μL phosphate buffer was added to 10 mg of H/D/M in 500 μL of phosphate buffer. The reagents were incubated on a shaker

(600 rpm) for 1 hour at 20°C, and pH 8. Afterward, the particles were purified and dissolved in 500 μL of purified water. The antibody was thiolated in PBS. Next, 250 μg of the purified and thiolated antibody (in 500 μL of purified water) was added to H/D/M suspension. Finally, the nanoparticles were incubated with the thiolated antibody for 12 hours and purified via centrifugation (12,000 rpm, 30 min, x3).

Characterization of HSA NPs and C-H/D/M NPs

The morphologic characteristics of HSA, H/D/M, and C-H/D/M were observed by transmission electron microscope (TEM). The size and zeta potential of the nanoparticles were measured by dynamic light scattering (DLS) using a Zetasizer. Briefly, nanoparticles were dispersed in deionized water (1 mg/mL), and sonicated for 5 min in an ice bath. The size was measured using a 1/300 (v/v) diluted nanoparticle suspension. The measurement was performed at 25 °C and done in triplicate. A dialysis assay was utilized to evaluate the release of DOX from C-H/D/M; the procedure is detailed in the Supporting Information 1.1.

Stability Determination

The particle size and PDI of the nanoparticles was determined within one month after synthesis. First, 7.5 μL of naked siMDR1 (0.075 nmol siMDR1) and 37.5 μL of C-H/D/M (0.075 nmol siMDR1) were precisely measured via an anti-RNase A degradation assay. Next, the samples were co-incubated with an equal volume of RNase A solution (0.1 mg/mL) at 37 °C for 30 minutes. Then, 5 μL EDTA solution (5 mM) was carefully added to stop the degradation at different set time points. Proteinase K (0.4 mg/mL, 200 mL) was used to displace siRNA from the C-H/D/M. Finally, an agarose gel retardation assay was used for stability detection.

Uptake of C-H/D/M NPs and Cell Viability

Cellular Uptake of Cy5 Labeled siRNA in MCF-7/ADR Cells by Confocal Microscopy

The cellular uptake of C-H/D/M was imaged using confocal laser scanning microscopy. Briefly, $5*10^4$ MCF-7/ADR cells were seeded into 20 mm confocal dishes and cultured in complete RPMI 1640 medium overnight. After cells were attached to the dishes, 1 mL of serum-free medium containing DOX, HSA/DOX (H/D), H/D/M, C-H/D/M, and Lipo^{TM}2000/siMDR1/DOX were added in order to transfect the cells for an additional 4 hours. Following the incubation period, the media was removed and cells were washed three times using 1 mL of a PBS solution. 1 mL of Hoechst 33342 (4 μg/mL) was added carefully into the dishes to stain the cell nuclei at 37°C for 20 minutes. Then, the liquid was discarded, and cells were washed twice with PBS solution. The intracellular location of MDR1 siRNA and DOX was captured by a confocal laser scanning microscope and analyzed using Leica CLSM software. The experiment was repeated three times, and a representative image of a single experiment has been provided.

Cell Culture and Cytotoxicity Assays in vitro

The MTT assay was used to evaluate the cytotoxicity of the HSA NPs and the C-H/D/M nanoparticle. MCF-7/ADR cells were plated at 4*104 cells/well in a 96-well plate and cultured for 24 h. The complete RPMI 1640 media was used as a blank control. For cytotoxicity of the HSA NPs, the cell were treated with 100 mL HSA NPs with different concentrations (0.1, 0.2, 0.5, 0.8, 1.0, 2.0, 4.0, and 6.0 mg/mL). The cells were then incubated with fresh media containing 0.5, 1, 5, 15, and 30 nM of HSA, DOX, H/D, H/D/M, C-H/D/M, and LipoTM2000/siMDR1/DOX (solution: 20 μL/well) for the anti-proliferation assay of the C-H/D/M at 37 °C for 6 hours. All the groups were incubated for another 44 hours. Then, 25 μL of an MTT solution (5 mg/mL) was added. After the incubation, the media was removed and replaced with 150 μL dimethyl sulfoxide (DMSO). The results were collected and analyzed at a wavelength of 570 nm using a microplate reader. In addition, migration and invasion was analyzed using Transwell filters. (see the Supporting Information 1.2). All experiments were repeated 3 times.

Cell Apoptosis and Gene Silencing Effect of C-H/D/M

Reverse Transcriptase Quantitative Polymerase Chain Reaction (RT-qPCR) Assay

Quantitative real time PCR was used to evaluate the MDR1 mRNA level in MCF-7/ADR cells treated with C-H/D/M. Before starting the study, MCF-7/ADR cells ($2*10^5$ cells/well) were seeded in six-well dishes and transfected with DOX, H/D, H/D/M, C-H/D/M, and Lipo^{TM}2000/siMDR1/DOX in media without FBS for 4 hours. Complete RPMI 1640 media was used as the blank control. After 4 h, the media was replaced with complete media and all wells were cultured for another 44 h. According to the product instructions, MCF-7/ADR cells were harvested and the total RNA in each well was

extracted using a Trizol reagent. The concentration of the total RNA was analyzed via a Nanodrop-1000 spectrophotometer. High-Capacity RNA-to-cDNA Kit was used to synthesize cDNA. The cDNA (80 ng) was determined by the 7500 Real-time PCR System. The Ct value was calculated using the delta-delta Ct ($2^{-\Delta\Delta Ct}$) method. Every experiment was repeated three times.

Gene Silencing Efficiency of C-H/D/M on Protein Level

The cellular protein levels were measured by ELISA. First, MCF-7/ADR ($2.0*10^5$ cells/well) were seeded into six-well plates. After culturing the cells overnight, the media was replaced with siMDR1, H/M, H/D/M, C-H/D/M, or Lipo^{TM}2000/siMDR1/DOX for 4 hours. After a 4 h incubation, all media in each well was replaced with complete media and all the cells were cultured for another 44 h. The cells were then scraped with a spatula. The suspension was centrifuged (125 g, 4 °C) for 10 min. A BCA Protein Quantification Kit was used to measure the protein concentration. A human MDR1 ELISA kit was used to measure the amount of P-gp in accordance with the manufacturer's instructions. The experiment was repeated three times.

Intracellular ATP Level Assay

MCF-7/ADR cells were seeded into a 6-well plate (500,000 cells per wells) and incubated for 24 hours at 37 °C. All the plates were treated with DOX, H/D, H/D/M, C-H/D/M, or Lipo^{TM}2000/siMDR1/DOX. The ATP concentration was determined using a luciferin-luciferase-based ATP luminescence assay kit as instructed by the manufacturer. The experiment was repeated three times.

Apoptosis Analysis Using Flow Cytometry

The above transfected MCF-7/ADR cells from the different groups were used to perform the apoptosis analysis using a fluorescein isothiocyanate (FITC)-labeled Annexin V (Annexin-V-FITC) and Propidium Iodide (PI) double staining. Briefly, $2*10^5$ cells in a 6-well plate were incubated with complete media, DOX, siMDR1 + DOX, H/D/M and C-H/D/M for 48 hours. After washing 3 times with cold PBS, the cells from each plate were collected. Annexin-binding buffer, 5 μL Annexin-V-FITC and 5 μL PI working solution were added to each cell suspension. Then, cellular apoptosis was observed by flow cytometry. Each experiment was performed in triplicate, and a representative picture was given.

Tumor Inhibition of C-H/D/M in vivo

BALA/c SPF mice (4-week-old, 18–22 g) were obtained from the Animal Department of the Capital Medical University. All animal studies were performed in accordance with the Health Guidelines of the Capital Medical University. To further evaluate the therapeutic effects of C-H/D/M in vivo, 50 female nude mice were injected with an MCF-7/ADR cell suspension (approximately $2*10^7$/mL cells) into the left armpit. All mice were housed in sawdust-lined cages with constant temperatures (22–25°C) and suitable humidity (50 ± 2.0%). When the tumor (volume (mm^3) = length * width^2/2) grew to approximately 600 mm^3, the tumor-bearing mice were randomly divided into 5 groups (n =8): normal saline (NS), DOX (1.2 mg/kg), DOX+siMDR1 (contain 1.2 mg/kg DOX and 0.8 μg/kg siRNA), H/D (contain 1.2 mg/kg DOX), H/D/M (contain 1.2 mg/kg DOX) and C-H/D/M (contain 1.2 mg/kg DOX). Then once every other day via intravenous injection the mice were treated with their corresponding therapeutic regimen or NS. The size of the tumor was measured every other day. After 10 days, tumor xenograft, brain, liver, spleen, heart, and kidneys were resected and collected for further pathological analysis with hematoxylin and eosin (H&E).

Tumor Targeting Ability of C-H/D/M

To evaluate the distribution of C-H/D/M, fluorescent images of each mouse were collected using the in vivo Imaging System FX Pro. The tumor-bearing mice were randomly divided into 3 groups and NS, H/D/M, and C-H/D/M was administered intravenously. After the mice were anesthetized with 2% isoflurane, florescent sagittal images were recorded at times 0.5 h, 2 h, 5 h, and 8 h.

In vivo Safety Evaluation

3mL of venous whole blood was obtained via a rat orbital puncture. The blood was centrifuged at 1000 rpm for 10 min, the red blood cells were collected and washed with PBS buffer three times, and a 2% (v/v) red blood cell suspension was prepared. Next, a 100 mL of the various drug concentrations were incubated with 900 μL of the red blood cell suspension and shaken slowly at 37 °C for 1 h. The sample was then centrifuged at 3000 rpm for 10 min and the supernatant was obtained and added to a 96-well plate. The absorbance value of the sample was measured at 540 nm and read by a microplate reader. All mice were euthanized on the 15th day after the first injection,

and blood samples were collected from all mice. The indicators for the functions of kidney and liver were measured using a blood biochemical autoanalyzer and a complete blood panel from healthy control and treated mice were tested.

Statistical Analysis

A two-sided Student's *t*-test and the one-way ANOVA were used to analyze the differences between groups. All numerical experimental values were collected from three separate experiments and expressed as means ± standard deviation (SD). A p-value < 0.05 was considered to be significantly different.

Result

Prescription Optimization of HSA NPs

The single factor experiments were carried out in order to evaluate the influence of the six factors on the preparation of HSA NPs (Figure 2). The results suggest that the HSA concentration, pH value, and volume and speed of ethanol addition were the most significant factors for HSA NPs preparation while stirring rate and volume of glutaraldehyde had little influence on the diameter and PDI of the HSA NPs. The four factors (HSA concentration, pH value, and volume and speed of ethanol addition) were selected for multi-factor analysis in order to obtain the optimal prescription for HSA preparation. Five levels for each factor were designed by the CCD-response surface methodology (CCD-RSM), and a total of 30 assays were generated by the Design Expert (Table 1). The optimal preparation of HSA NPs was calculated, and determined to be 19.409 mg/mL for the HSA concentration, 8.609 for the pH value, 4.134 mL for the volume of ethanol, and 1.503 mL/min for the speed of ethanol addition (Figure 3).

Next the optimal prescription was applied for HSA NPs preparation. The particle size, PDI, and zeta potential of the prepared HSA NPs were 178.280 ± 1.552 nm, 0.044 ± 0.006, and −35.760 ± 0.115, respectively, which had no significant differences with the predicted ones (Table 2). The results confirmed that the CCD-RSM had an excellent prediction for the HSA NPs preparation and was a promising method for optimizing the preparation.

Preparation and Characterization of C-H/D/M NPs

The optimal prescription obtained was applied for the preparation of DOX and siMDR1 loaded HSA NPs. In order to investigate the most suitable ratio for loading DOX and siMDR1 with the HSA NPs, DOX or siMDR1 with different concentrations were mixed with HSA to prepare either DOX or siMDR1 loaded HSA NPs. As shown in Figure 4A, in preparation of DOX loaded HSA NPs (HSA/DOX NPs), the drug loading capacity (DLC) and entrapment efficiency (EE) increased with the mass ratio (mg/mg) of DOX to HSA. However, the DLE and EE of HSA/DOX NPs remained the same as the mass ratio increased to over 2:20. However, the ratio of DOX to HSA was determined to be 2:20 for the preparation of DOX and siMDR1 co-delivered HSA NPs. The agarose gel retardation assay was performed to determine the optimal siMDR1loading concentration. The bands of siMDR1 diminished gradually as the weight ratio (μg/mg) of siMDR1: HSA increased. The band completely disappeared when the ratio reached 0.8:1, indicating that all of the siMDR1 was loaded into the HSA NPs (Figure 4B). According to the results, the ratio of DOX to HSA was determined to be 0.8: 1 for the preparation of DOX and siMDR1 co-delivered HSA NPs.

After preparing the DOX and siMDR1 co-delivered HSA NPs, the nanoparticles were functionalized with cetuximab in order to obtain the C-H/D/M NPs. C-H/D/M NPs were characterized by DLS and TEM. The hydrodynamic radius of HSA NPs was 161.8 ± 1.68 nm as shown in Figure 4C, and the hydrodynamic radius of the C-H/D/M NPs increased to 174.9 ± 1.30 nm, due to the drug loading and cetuximab functionalization. TEM images revealed that the HSA NPs remained spherical and uniform after carrying drugs and functionalizing the NP's with cetuximab (Figure 4D).

The storage stability of C-H/D/M NPs was determined by measuring particle size and PDI of the nanoparticles within one month after synthesis. The results indicated that the diameter and PDI remained almost unchanged during the stability test proving the excellent storage stability of the nanoparticles (Figure 4E). The dispersion stability of the C-H/D/M NPs was analyzed in different solutions (water, PBS, and RPMI-1640 medium). As shown in Figure 4E, the nanoparticles can be dispersed homogeneously in all conditions. Degradation by RNase A in vivo is one of the biggest barriers for siRNA delivery,[46] and the siRNA protection effect of the C-H/D/M NPs was determined using a gel retardation assay. The band of naked siMDR1 completely disappeared after incubation with RNase A for 5 min. However, the band of siMDR1 remained nondetectable

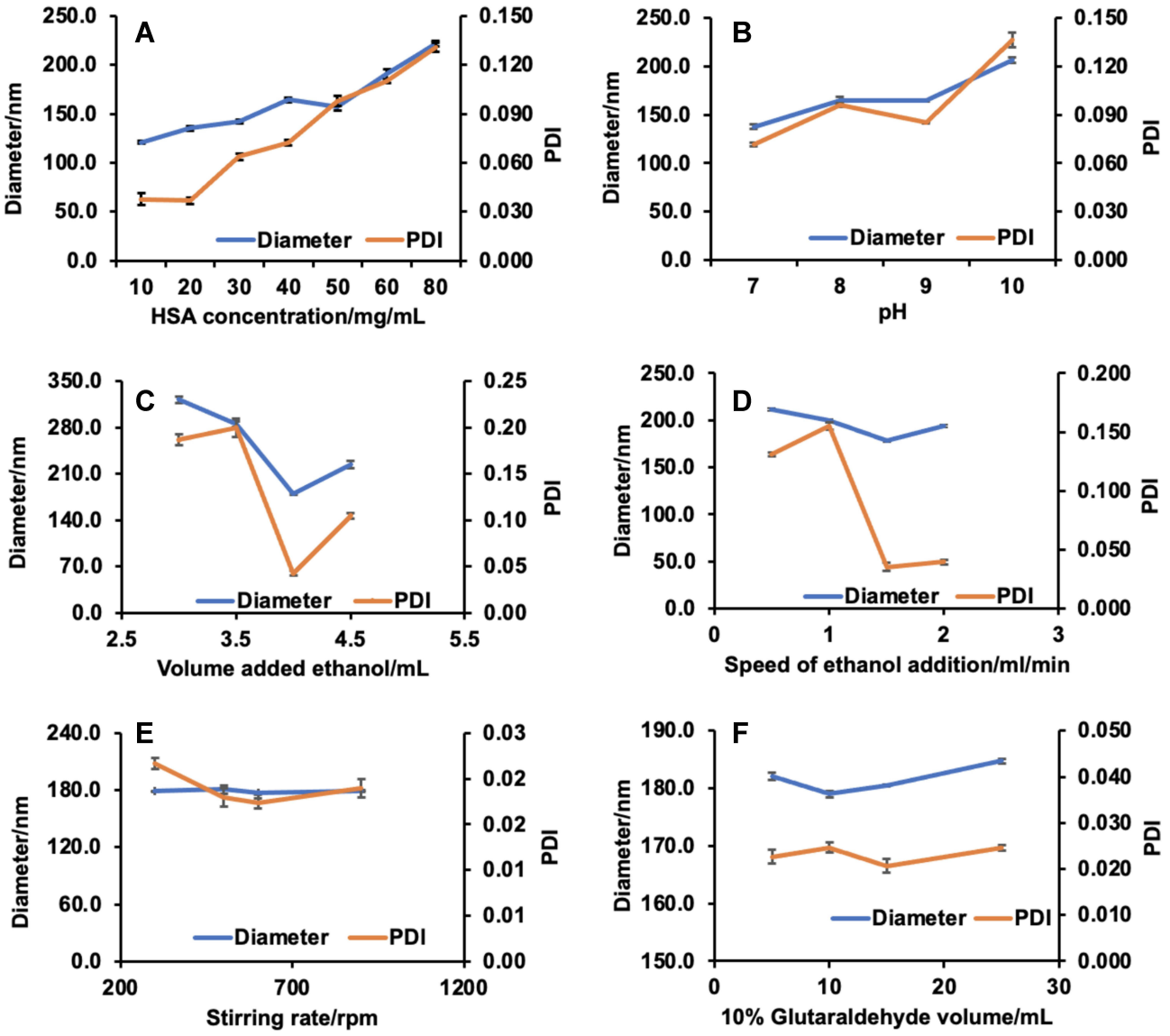

Figure 2 Six single factors influence of the diameter and PDI and prescription optimization of HSA NPs and. (**A**) HSA concentration. (**B**) pH value. (**C**) Volume added ethanol. (**D**) Speed of ethanol addition. (**E**) Stirring rate. (**F**) 10% glutaraldehyde volume. (n=6).

for as long as 5 h. The superior protection effect of the C-H/D/M NPs guarantees the activity of siMDR1 in vivo as well as the ability to increase the amount of siMDR1 delivered to the site of the tumor; thus, producing a significant gene silencing effect (Figure 4F). A dialysis assay was applied to evaluate the release of DOX from the C-H/D/M. The cumulative release of DOX at 216 hours at pH 7.4 and pH 5.0 was 59.37% ± 2.66% and 79.42% ± 0.16%, respectively. It was proven that, compared to the tumor environment (pH 5.0), the amount of C-H/D/M release reduced significantly. (Supporting Information and Figure S1)

Cell Inhibition Effect of C-H/D/M NPs

The drug resistance of MCF-7/ADR was confirmed using an MTT assay (Figure 5A). The IC_{50} of DOX on MCF-7 cells was 5.25 μmol/L; however, DOX does not inhibit the cell proliferation of the MCF-7/ADR cells even when the concentration of DOX was as high as 5 μmol/L. The safety of HSA as a gene carrier was also tested by an MTT assay (Figure 5C). The viability of MCF-7/ADR cells remained over 90%, even when the concentration of HSA reached 6 mg/mL. The results suggested that HSA is a safe material for drug delivery. In order to reverse the resistance of MCF-7/ADR cells to DOX, HSA nanoparticles were

Table 1 Factors and Five Different Levels in CCD Design Experiment. HSA Concentration, pH Value, Volume of Ethanol and Speed of Ethanol Addition Were Selected for Multi-Factor Analysis to Obtain the Optimal Prescription for HSA Preparation. 5 Levels for Each Factors Were Designed by CCD-Response Surface Methodology (CCD-RSM)

Factors	Symbol	Coded Levels				
		−2	−1	0	1	2
HSA concentration/ mg/mL	A		10	30	50	70
pH value	B	5.5	7	8.5	10	11.5
Volume added ethanol/mL	C	2.25	3	3.75	4.5	5.25
Speed of ethanol addition/mL/min	D		0.5	1.25	2	2.75

prepared in order to co-deliver DOX and siMDR1; the nanoparticles were functionalized with cetuximab for tumor targeted drug delivery. The drug resistance reversing effect and cellular targeting effect of the C-H/D/M NPs in vitro were determined by both cellular uptake and MTT assay. As shown in Figure 5B, the uptake of DOX could not be significantly increased when it was loaded in HSA nanoparticles. However, after co-delivery with siMDR1 by the HSA nanoparticles, the amount of DOX in the cells was significantly enhanced and was attributed to the P-gp protein silencing effect of siMDR. Furthermore, the fluorescence of Cy5-siMDR1 in the MCF-7/ADR cells treated with C-H/D/M NPs was more intense than the cells treated with H/D/M, indicating the cellular targeting effect of C-H/D/M in vitro.

Considering the above results, it is hypothesized that the C-H/D/M NPs can reverse the resistance of DOX on MCF-7/ADR cells, therefore significantly increasing the cytotoxicity of DOX. However, an MTT assay was performed to test the cytotoxicity of the C-H/D/M NPs on MCF-7/ADR cells (Figure 5D). The cell viability of DOX and the siMDR1 treated group was similar to that of the DOX treated group suggesting that the naked siMDR1 cannot reverse the resistance of DOX since it could not be effectively delivered into the cells. When DOX and siMDR1 were loaded into the HSA NPs together, the cell viability of MCF-7/ADR cells was significantly reduced. Moreover, HSA/DOX/siRNA had an equal tumor inhibition effect compared to DOX + Lipo/siRNA, which served as a positive control. When the concentration of siMDR1 reached 30 nM, the cell viability of the H/D/M treated group and the DOX+ Lipo/siMDR1 treated group was 46.68% ± 0.71% and 47.31% ± 0.26%, respectively confirming the excellent anti-tumor effect of H/D/M by reversing the resistance of DOX in vitro. However, when the concentration of siMDR1 reached 30nM, the cell viability for the C-H/D/M NPs treated group was 38.93% ± 0.05%, which was significantly decreased compared to the H/D/M NPs treated group. This result demonstrates that NPs functionalized with cetuximab enhance the antitumor effect of H/D/M by promoting the cellular uptake of the nanoparticles. A transwell assay was performed to evaluate the effects of C-H/D/M on cell migration and invasion. The results indicate that C-H/D/M inhibits the migration and invasion of MCF-7/ADR cells (Supporting Information and Figure S2).

Cell Apoptosis and Gene Silencing Effect of C-H/D/M

As a widely used anti-tumor drug, DOX exerts its anti-tumor effect by promoting cell apoptosis.[47] In order to investigate the anti-tumor mechanism of C-H/D/M, cell apoptosis analysis was performed by FCM (Figure 6A and C). For DOX and the siMDR1 co-treated group, the percentage of cells in early and late apoptotic phases (Q2 and Q4) was 20.23% ± 3.15%. However, the percentage of apoptotic cells increased significantly to 32.60% ± 2.83%, when DOX and siMDR1 were co-delivered via HSA nanoparticles. Furthermore, the percentage was further increased to 39.66% ± 1.60%, when H/D/M was modified with cetuximab. These results strongly suggest that C-H/D/M inhibits tumor cell proliferation by co-delivering DOX and siMDR1 into MCF-7/ADR cells, enhancing cellular apoptosis; thus, promoting the effect of DOX.

In order to investigate if the superior anti-tumor effect of C-H/D/M on MCF-7/ADR cells was attributed to the regulation of drug resistant genes, the gene silencing effect of C-H/D/M was investigated at both the mRNA and protein levels. As shown in Figure 6D, naked siMDR1 does not down-regulate the expression of either MDR1 mRNA or the P-gp protein. In contrast, the Cex-HSA/siMDR1 NP treated group had significantly decreased mRNA and protein expression levels, showing a 59.67% ± 3.1 and 65.42% ± 2.4% decrease in expression, respectively. The positive control group (Lipo/siMDR1) had similar mRNA and

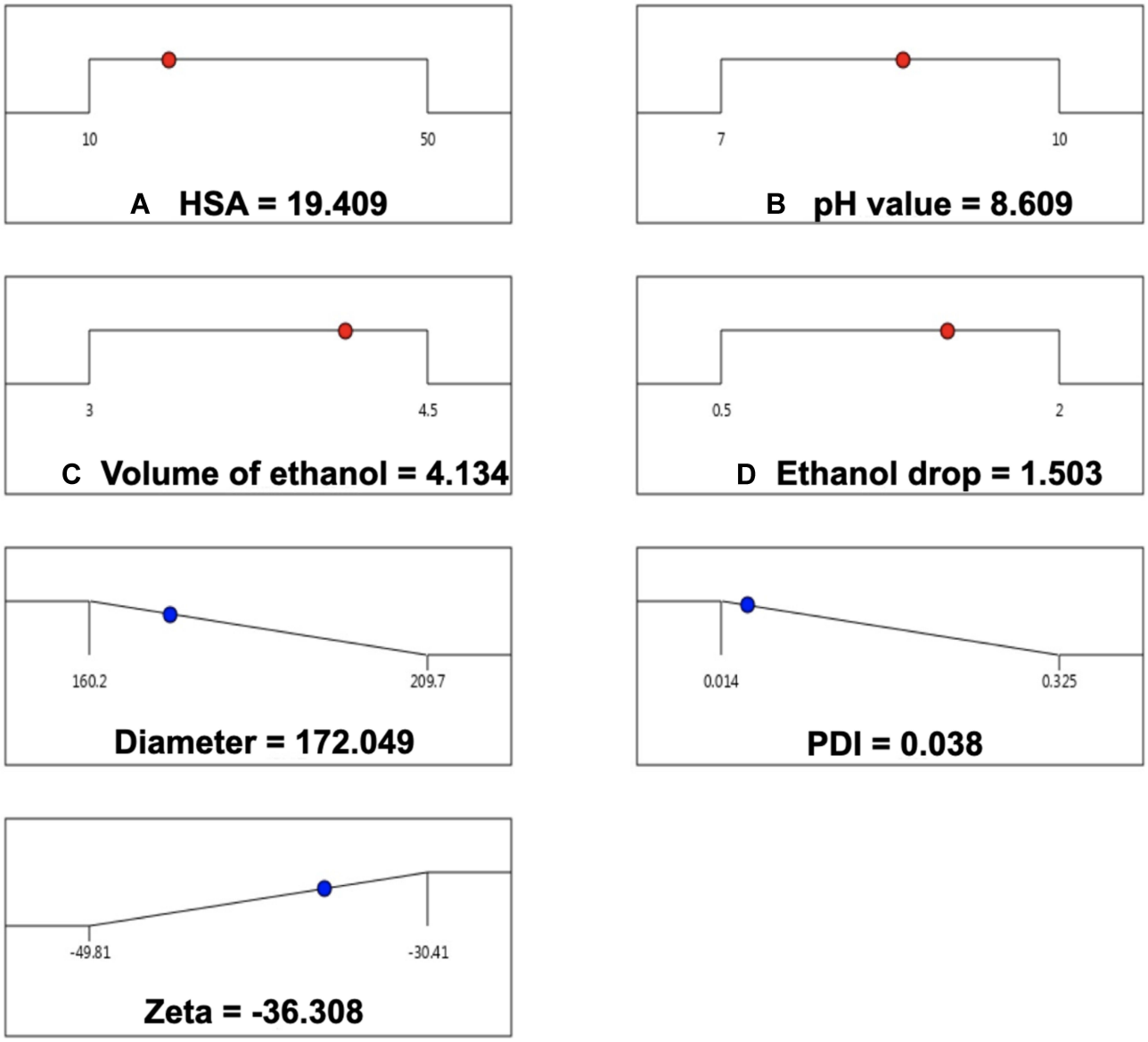

Figure 3 The optimal preparation of HSA NPs. The particle size, PDI and zeta potential of prepared HSA NPs were 178.280 ± 1.552 nm, 0.044 ± 0.006 and −35.760 ± 0.115 separately.

protein levels compared to the Cex-HSA/siMDR1 NP treatment group of 59.67% ± 2.1 and 63.92% ± 1.5%, respectively. Moreover, co-loading with DOX did not influence on the gene silencing effect of siMDR1, and Cex-HSA /siMDR1/DOX NPs had an equal mRNA and protein down-regulation effect with Cex-HSA/siMRD1 (Figure 6E).

It is well known that P-gp belongs to the adenosine 5′-triphosphate (ATP)–binding cassette (ABC) transporters.[48] As a drug efflux pump P-gp is over-expressed on MCF-7/

Table 2 Comparison of Experimental Actual Value and Predicted Value

Evaluation Index	Predicted Response	Observed Response	Predicted Error
Diameter/nm	172.049	178.280 ± 1.552	0.035
PDI	0.038	0.044 ± 0.006	0.136
Zeta/mV	−36.308	−35.760 ± 0.115	0.015

Notes: There were no significant differences with these predicted values. The results confirmed that CCD-RSM had an excellent effect for HSA NPs preparation.

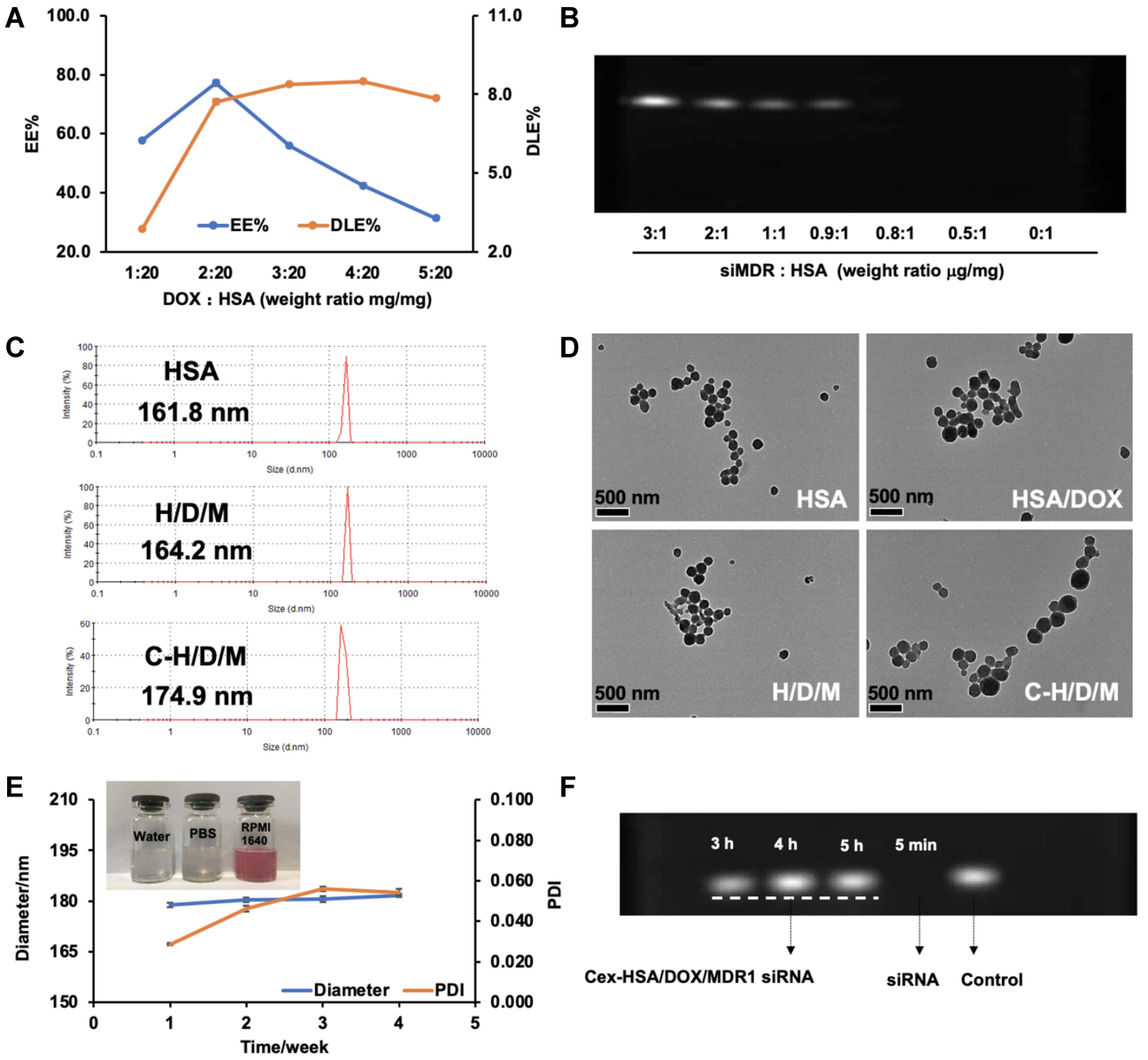

Figure 4 Preparation and Characterization of Cex-HSA/DOX/siMDA1 NPs. (**A**) The drug loading and encapsulation efficiency of HSA/DOX with different mass ratios (n=3). (**B**) Agarose gel retardation assays of siMDR1 complexed with HSA/DOX. (**C**) The Diameter of HSA, H/D/M and C-H/D/M. (**D**) TEM images of the HSA, HSA/DOX, H/D/M and C-H/D/M. (**E**) Dispensability, stability, particle size, PDI. (**F**) Agarose gel retardation assay of anti-RNase A stability diagram of C-H/D/M.

ADR cells' membrane and depends on cellular energy for drug transportation.[49] Intracellular levels of ATP are an indicator of P-gp function. Thus, the ATP levels within MCF-7/ADR cells were evaluated as a function of P-gp activity. As shown in Figure 6B, the total amount of ATP in the H/D/M treated MCF-7/ADR cells was 51.51% ± 0.24%, which was equal to that in the DOX and Lipo/siMDR1 co-treated cells. Moreover, the total amount of ATP in C-H/D/M treated cells was 45.56% ± 0.03%, which is significantly lower than that in the H/D/M treated cells ($P < 0.01$). This result confirmed the targeting effect of C-H/D/M.

Overall, all of the results demonstrated that C-H/D/M reverses the drug resistance of MCF-7/ADR cells through the inhibition of the expression of P-gp protein as well as the down-regulation of cellular ATP levels.

Tumor Growth Inhibitory Activity in vivo

The tumor inhibition effect of C-H/D/M was studied in MCF-7/ADR xenograft models. Tumor volumes of the NS, DOX, and DOX + siMDR1 groups show no significant difference ($P > 0.05$); however, they were higher than the H/D/M and C-H/D/M groups (Figure 7A and B). The

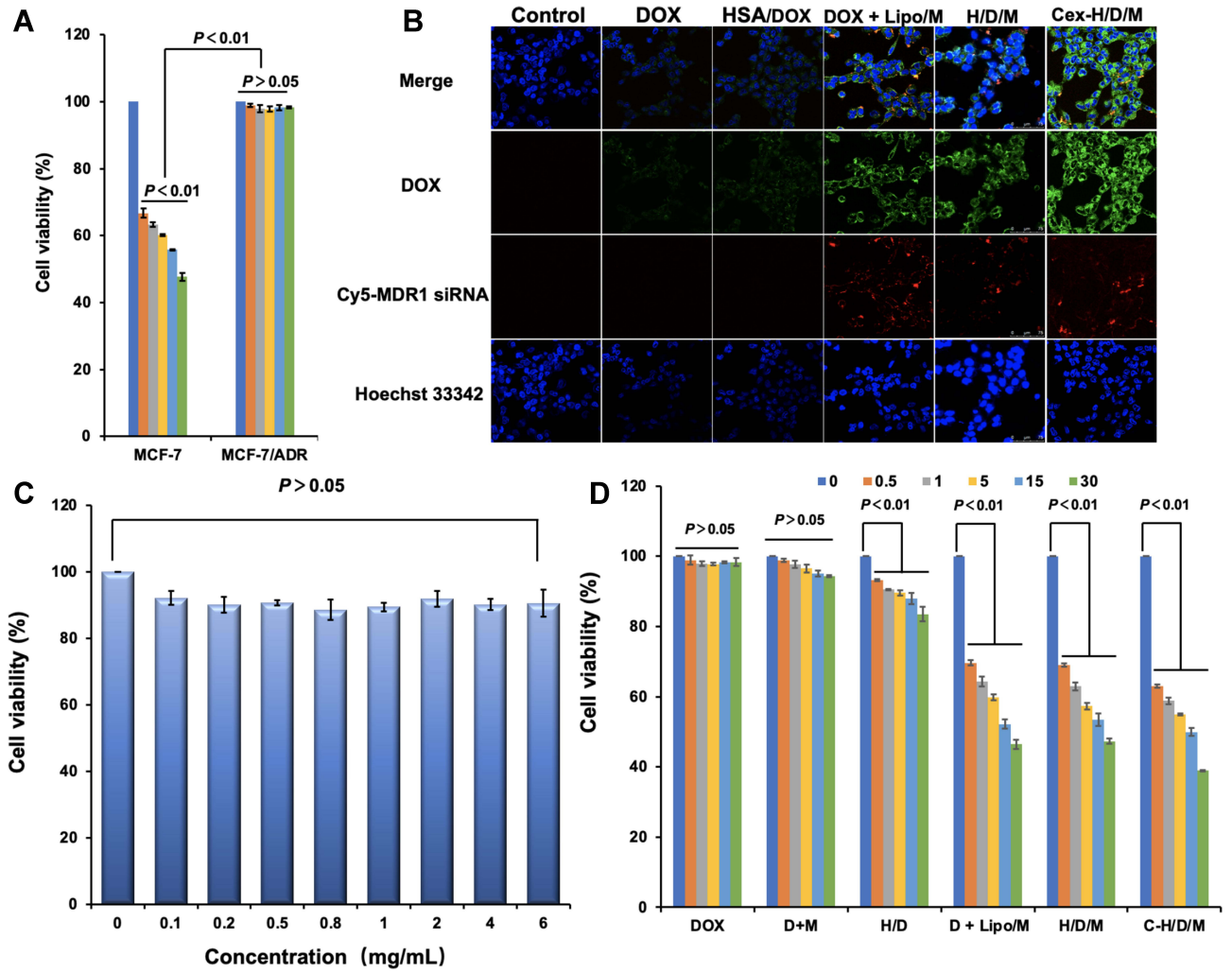

Figure 5 Intracellular delivery, safety of HSA and antiproliferation effect of C-H/D/M in vitro. (**A**) The drug resistance of MCF-7/ADR using MTT assays. (**B**) Confocal images of MCF-7/ADR cells treated with DOX, HSA/DOX, DOX+ Lipo/siRNA, H/D/X and C-H/D/M; siRNA was labled with Cy5 fluorescent molecule (red) to show the amount of siRNA into cells, the DOX were green and Hoechst 33342 (blue) for cell nucleus. (**C**) The cytotoxicity assays of HSA NPs on MCF-7/ADR cells. (**D**) Anti-proliferation effect of C-H/D/M in MCF-7/ADR cells. The data were presented as the mean ± SD, n=3.

tumor volumes decreased with time and the tumor inhibitory rate of the C-H/D/M group (54.05% ± 1.25%) was significantly higher than that of H/D/M (38.07% ± 4.04%), DOX (5.71% ± 5.43%), and DOX + siMDR1 (5.39% ± 3.82%) groups. Hematoxylin and eosin (H&E) staining revealed the histological changes of the tumor tissue after treatment with C-H/D/M. (Figure 7C) The cytoplasm of the normal tumor cells and the blood vessels were clearly observed. After treatment with C-H/D/M, the tumor cells became sparse, the blood vessels were difficult to identify and the intercellular space increased in size, which are the typical characteristics of necrosis. The results revealed that Cex-HSA/DOX/MDR1 damages tumor tissue, inhibits the formation of blood vessels, and causes hemorrhage at the site of the tumor. In addition, according to the ratios of organ to body weight, C-H/D/M does not cause damage to the vital organs (Figure 7D).

In vivo Imaging

As previously reported, the HSA molecule has passive and active targeting properties.[50] The tumor-targeting abilities of systemically delivered DOX and siMDR1 were investigated in an MCF-7/ADR tumor xenograft nude mouse model using a fluorescent imaging assay. Cy5 labeled siMDR1 was used to trace the distribution of siMDR1 in vivo. The tumor site shown in Figure 8, shows that the Cex-HSA/DOX/MDR1 group had a continuous fluorescent signal in tumor areas and the signal from this group was the most intense compared to the other treatment groups. Naked siRNA was primarily distributed in the

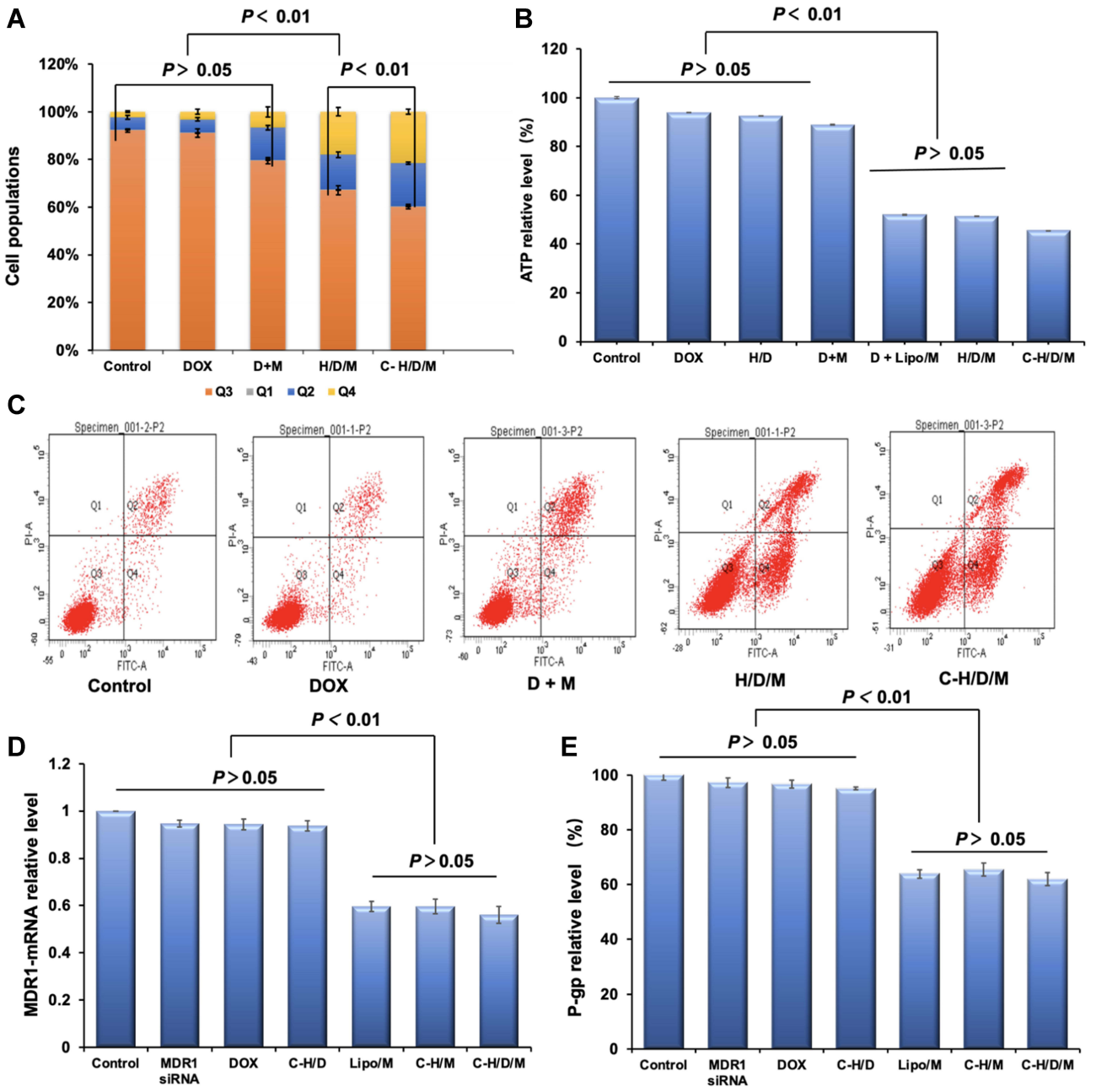

Figure 6 Cell apoptosis of MCF-7/ADR cells treated by C-H/D/M for 48 h and in vitro gene silencing effect. (**A**) Statistical chart of cell cycle distribution of MCF-7/ADR cells treated with different treatment groups. (**B**) The ATP level in MCF-7/ADR cells of different groups. (**C**) Distribution of MCF-7/ADR cell apoptosis detected by flow cytometry in different treatment groups. (**D**) MDR1-mRNA levels of the MCF-7/ADR cells treated with different siMDR1 formulations were tested by RT-PCR. (**E**) P-gp levels of the MCF-7 cells treated with different siMDR1 formulations were tested by ELISA assay. The cells with no treatment was considered as a control. The data were presented as the mean ± SD, n=3.

liver and was quickly metabolized. Furthermore, at each observation time point, the signal intensity of the tumor site in each group is as follows DOX + siMDR1 < H/D/M< C-H/D/M. The results show that the HSA nanoparticles effectively delivered siMDR1 and DOX to the site of the tumor, and that cetuximab plays a role in targeting.

In vivo Safety Evaluation

In this study, we used an endogenous biological macromolecule-HSA which has the advantages of biodegradability, non-toxicity, and non-immunogenicity.[51]

First, the main organs were stained with H&E to investigate the organ toxicity of C-H/D/M. As shown in

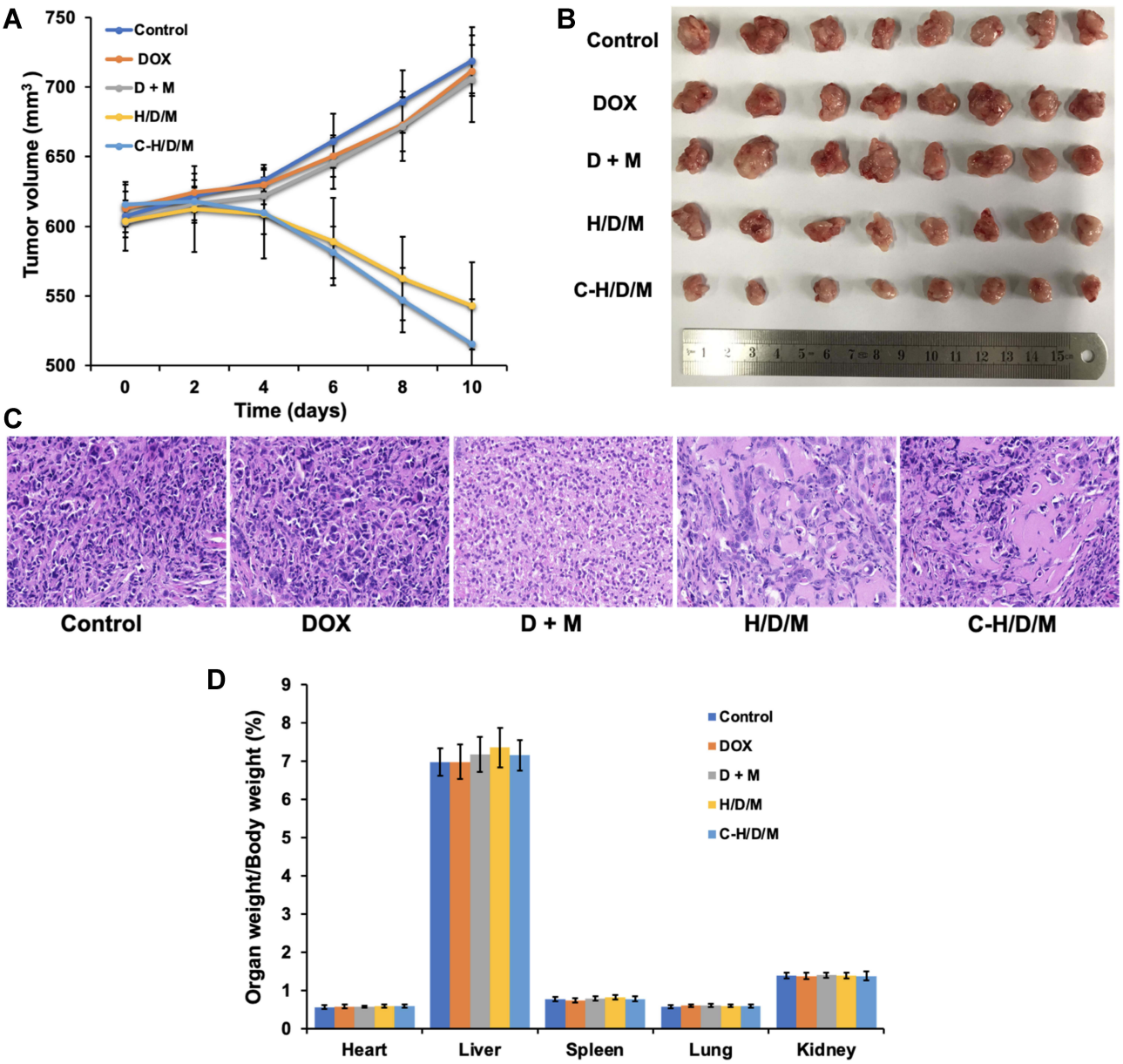

Figure 7 In vivo tumor therapeutic efficiency of C-H/D/M. (**A**) Tumor volume changes of mice were measured every two days. (**B**) Image of tumors collected from the mice on the day after the last injection. (**C**) H&E staining of MCF-7/ADR tumor tissues in nude mice injected with NS (Control), DOX, DOX+siMDR1, H/D/M, C-H/D/M. (100×). (**D**) The ratios of organ weight to body weight. The data were presented as the mean ± SD, n=6.

Figure 9A, there were no obvious pathological features in the heart, liver, spleen, lungs, and kidneys of each group, suggesting that C-H/D/M had no apparent toxicity to the main organs in vivo. Figure 9B shows the hemolysis percentages of the different treatments. The hemolysis percentages of the HSA NPs and C-H/D/M were 2.15 ± 1.05% and 1.74 ± 0.96%, respectively, and were lower than observed in the DOX treatment group. Thus, it can be concluded that C-H/D/M possess better blood compatibility. We observed no obvious hepatic or renal toxicity introduced by these nanoparticles, as indicated by the normal values of the liver and kidney function biomarkers. Hematology analysis revealed no significant differences in the blood parameters between the treated and control groups (Figure 9C–F). The results indicated no significant difference in blood indexes between the control and the treatment groups (Table 3).

Discussions

Chemotherapy is a vital treatment for breast cancer. The combined use of RNA interference and chemotherapeutic drugs has attracted scientific interest and has been widely

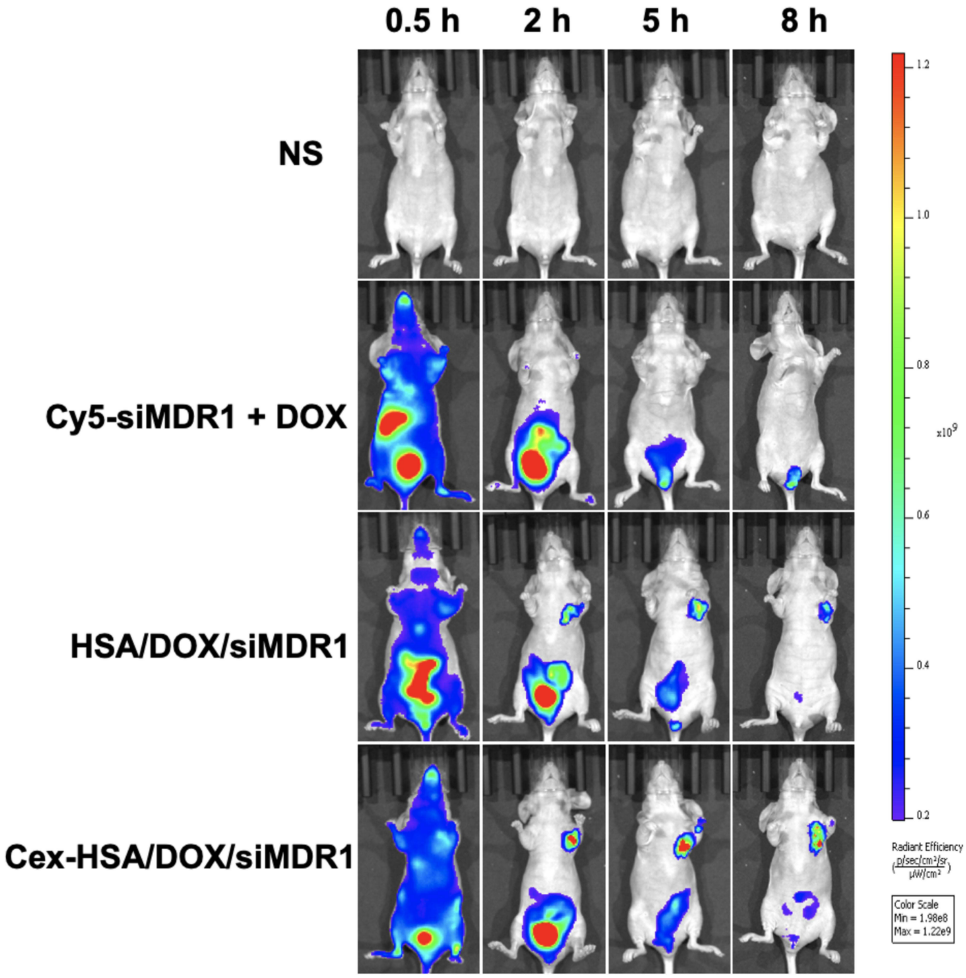

Figure 8 In vivo fluorescence image of different groups injected into tail of BALB/c nude mice. Images were taken at different time points after tail vein injection.

used in the treatment of cancer. Previous studies have demonstrated that mesoporous silica nanoparticles carrying MDR1-siRNA and DOX effectively inhibit expression of the MDR1 gene and cures tumors in human oral cancer cells.[20] Our study synthesized a carrier with many biocompatibility advantages, such as non-immunogenicity, biodegradability and non-toxicity.

Human serum albumin (HSA) is an endogenous biomacromolecule and has been shown to be effective in the delivery of anti-tumor drugs. In this research, CCD-RSM was used to optimize the prepared formula in order to synthesis the HSA NPs. The particle size, PDI, and zeta potential of the prepared HSA NPs were the same as the predicted particles indicating that this method had excellent predictability. The optimal formula was applied in the preparation of DOX and MDR1 siRNA co-loaded HSA NPs. TEM images and DLE revealed that the HSA NPs remained spherical and uniform after drug loading and cetuximab functionalization. The storage stability results indicated that the diameter and PDI remained unchanged during the stability observation period and protected the MDR1 siRNA from degradation by RNase A.

Our in vitro data demonstrated that the resulting nanoparticles not only exhibits excellent storage stability but also efficiently transfects MCF-7/ADR cells. The increased intracellular delivery of DOX via C-H/D/M is due to the targeting ability of cetuximab. Considering the PCR and ELISA results, C-H/D/M can effectively inhibit MDR1 gene expression in order to inhibit DOX efflux leading to apoptosis of the breast cancer cells. Furthermore, the data from the tumor model reveals that C-H/D/M dramatically decreases tumor size and changes the distribution of DOX. C-H/D/M inhibits tumor growth and induces cell death in tumor tissue without causing any cytotoxicity within the vital organs.

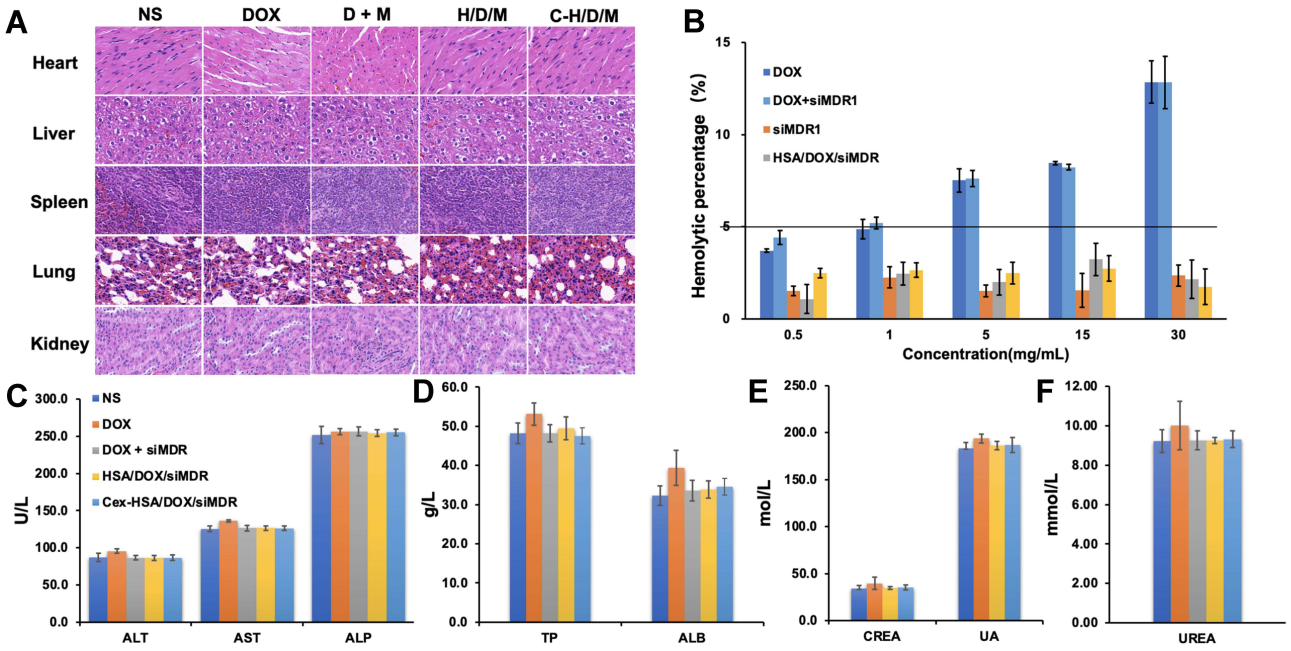

Figure 9 Biosafety of C-H/D/M in vivo. (**A**) H&E staining of the major organs from mice treated with NS (Control), DOX, DOX+siMDR1, H/D/M and C-H/D/M. (100×). (**B**) Hemolysis activity of C-H/D/M, hemolysis rate was evaluated in rat RBC. The data were presented as the mean ± SD, n=3. (**C**) Blood biochemistry data including liver function markers: ALT, AST, ALP. (**D**) Liver function markers: TB and ALB. (**E**) Kidney function markers: CREA, UA. (**F**) Kidney function markers: UREA. The data were presented as the mean ± SD, n=5.

In summary, these assays strongly indicate that HSA prepared using the optimal formula was an excellent delivery system, and it could enhance the DOX effect by promoting tumor targeting effect.

Conclusions

In summary, an HSA-based nanoparticle drug delivery system was successfully synthesized to co-deliver DOX and siMDR1 to drug resistant breast cancer cells. CCD-RSM, an effective prescription optimization method, was utilized to obtain the optimal HSA NP formulation. After functionalization with cetuximab, the delivery system was able to deliver DOX and siMDR1 simultaneously and effectively to breast cancer cells in vitro, and also successfully target the delivery system to the site of the tumor in vivo. C-H/D/M exhibited excellent stability under different conditions promoting the uptake of DOX and siRNA by the MCF-7/ADR cells. The in vitro antiproliferation assays showed that the down-regulation of MDR1-mRNA and P-gp had no significant differences compared to the Lipo^{TM}2000/siRNA positive control. The in vitro experiments proved that C-H/D/M

Table 3 Blood Routine Test

	Unit	NS	DOX	DOX + siRNA	H/D/M	C-H/D/M
WBC	10^9/L	3.7 ± 0.1	3.6 ± 0.1	3.7 ± 0.3	3.5 ± 0.2	3.3 ± 0.2
RBC	10^12/L	8.16 ± 0.57	8.04 ± 0.23	8.00 ± 0.25	7.94 ± 0.19	7.72 ± 0.30
HGB	g/L	146 ± 9	146 ±4	143 ± 3	145 ± 1	143 ± 4
HCT	%	44.7 ± 3.2	45.7 ± 1.6	44.8 ± 1.7	44.8 ± 1.5	45.3 ± 1.4
MCV	fL	53.5 ± 2.5	54.4 ± 1.5	54.2 ± 2.6	53.5 ± 1.2	54.1 ± 3.2
MCH	pg	17.5 ± 0.1	17.6 ± 0.2	17.9 ± 0.8	17.8 ± 0.3	17.7 ± 0.4
MCHC	g/L	333 ± 7	326 ± 4	328 ± 9	331 ± 6	326 ± 11
PLT	10^9/L	573 ± 22	562 ± 23	558 ± 20	559 ± 5	560 ± 13
PDW	fL	24.6 ± 3.4	23.4 ± 2.6	23.2 ± 1.1	23.2 ± 0.5	23.2 ±1.2

Note: The data were presented as the mean ± SD, n=5.
Abbreviations: RBC, red blood cell; HGB, hemoglobin; HCT, hematocrit; MCV, mean corpuscular volume; MCH, mean corpuscular hemoglobin; MCHC, mean corpuscular hemoglobin concentration; RDW, red blood cell distribution width; PLT, platelet; and WBC, white blood cell.

could suppress MCF-7/ADR cells proliferation through the promotion of apoptosis. Due to the active and passive targeting effect, C-H/D/M exhibited an excellent tumor targeting effect after in vivo administration. In addition, the animal studies suggest that the tumor inhibition of C-H/D/M was much higher than DOX alone. The toxicity and biosafety research in vitro and in vivo suggested that C-H/D/M was a safe and biocompatible material and showed no toxicity to the animal's vital organs. All of the results in this research provide an efficient method for designing HSA NPs and shows a novel drug delivery system with remarkable DOX and gene delivery abilities.

Acknowledgments

The authors gratefully acknowledge the support from Beijing Area Major Laboratory of Peptide and Small Molecular Drugs, Engineering Research Center of Endogenous Prophylactic of Ministry of Education of China, and Beijing Laboratory of Biomedical Materials. The authors thank AiMi Academic Services (www.aimieditor.com) for the English language editing and review services.

Author Contributions

All authors made a significant contribution to the work reported, whether that is in the conception, study design, execution, acquisition of data, analysis and interpretation, or in all these areas; took part in drafting, revising or critically reviewing the article; gave final approval of the version to be published; have agreed on the journal to which the article has been submitted; and agree to be accountable for all aspects of the work.

Funding

This work was supported by the National Natural Science Foundation (81502688), Beijing Natural Science Foundation Program and Scientific Research Key Program of Beijing Municipal Commission of Education (KM201810025019), and a basic-clinical key research grant (16JL72, 17JL67) from Capital Medical University, the Importation and Development of High-Caliber Talents Project of Beijing Municipal Institutions (2013–2015).

Disclosure

The authors declare no conflict of interest.

References

1. Blair S, Garcia M, Davis T, et al. Hexachromatic bioinspired camera for image-guided cancer surgery. *Sci Transl Med*. 2021;13(592). doi:10.1126/scitranslmed.aaw7067
2. Terrisse S, Derosa L, Iebba V, et al. Intestinal microbiota influences clinical outcome and side effects of early breast cancer treatment. *Cell Death Differ*. 2021;28(9):2778–2796. doi:10.1038/s41418-021-00784-1
3. Tian F, Zhang S, Liu C, et al. Protein analysis of extracellular vesicles to monitor and predict therapeutic response in metastatic breast cancer. *Nat Commun*. 2021;12(1):2536. doi:10.1038/s41467-021-22913-7
4. Zhang J, Wang N, Li Q, Zhou Y, Luan Y. A two-pronged photodynamic nanodrug to prevent metastasis of basal-like breast cancer. *Chem Commun (Camb)*. 2021;57(18):2305–2308. doi:10.1039/d0cc08162k
5. Zheng X, Zhao Y, Jia Y, et al. Biomimetic co-assembled nanodrug of doxorubicin and berberine suppresses chemotherapy-exacerbated breast cancer metastasis. *Biomaterials*. 2021;271:120716. doi:10.1016/j.biomaterials.2021.120716
6. Wan MM, Chen H, Da wang Z, et al. Nitric oxide-driven nanomotor for deep tissue penetration and multidrug resistance reversal in cancer therapy. *Adv Sci (Weinh)*. 2021;8(3):2002525. doi:10.1002/advs.202002525
7. Au KM, Balhorn R, Balhorn MC, Park SI, Wang AZ. High-performance concurrent chemo-immuno-radiotherapy for the treatment of hematologic cancer through selective high-affinity ligand antibody mimic-functionalized doxorubicin-encapsulated nanoparticles. *Acs Central Sci*. 2019;5(1):122–144. doi:10.1021/acscentsci.8b00746
8. Liu J, Ye Z, Xiang M, et al. Functional extracellular vesicles engineered with lipid-grafted hyaluronic acid effectively reverse cancer drug resistance. *Biomaterials*. 2019;223:119475. doi:10.1016/j.biomaterials.2019.119475
9. Liu J, Zhu C, Xu L, et al. Nanoenabled intracellular calcium bursting for safe and efficient reversal of drug resistance in tumor cells. *Nano Lett*. 2020;20:8102–8111. doi:10.1021/acs.nanolett.0c03042
10. He Y, Li X, Ma J, et al. Programmable codelivery of doxorubicin and apatinib using an implantable hierarchical-structured fiber device for overcoming cancer multidrug resistance. *Small*. 2019;15(8):1804397. doi:10.1002/smll.201804397
11. Das T, Anand U, Pandey SK, et al. Therapeutic strategies to overcome taxane resistance in cancer. *Drug Resist Updat*. 2021;55:100754. doi:10.1016/j.drup.2021.100754
12. Dallavalle S, Dobričić V, Lazzarato L, et al. Improvement of conventional anti-cancer drugs as new tools against multidrug resistant tumors. *Drug Resist Update*. 2020;50:100682. doi:10.1016/j.drup.2020.100682
13. Zhang L, Li Y, Wang Q, et al. The PI3K subunits, P110alpha and P110beta are potential targets for overcoming P-gp and BCRP-mediated MDR in cancer. *Mol Cancer*. 2020;19(1):10. doi:10.1186/s12943-019-1112-1
14. Wang S, Liu X, Chen S, et al. Regulation of Ca(2+) signaling for drug-resistant breast cancer therapy with mesoporous silica nanocapsule encapsulated doxorubicin/siRNA cocktail. *ACS Nano*. 2019;13(1):274–283. doi:10.1021/acsnano.8b05639
15. Haggag Y, Abu Ras B, El-Tanani Y, et al. Co-delivery of a RanGTP inhibitory peptide and doxorubicin using dual-loaded liposomal carriers to combat chemotherapeutic resistance in breast cancer cells. *Expert Opin Drug Del*. 2020;17(11):1655–1669. doi:10.1080/17425247.2020.1813714
16. Gu J, Fang X, Hao J, Sha X. Reversal of P-glycoprotein-mediated multidrug resistance by CD44 antibody-targeted nanocomplexes for short hairpin RNA-encoding plasmid DNA delivery. *Biomaterials*. 2015;45:99–114. doi:10.1016/j.biomaterials.2014.12.030

17. Tsouris V, Joo MK, Kim SH, Kwon IC, Won YY. Nano carriers that enable co-delivery of chemotherapy and RNAi agents for treatment of drug-resistant cancers. *Biotechnol Adv*. 2014;32(5):1037–1050. doi:10.1016/j.biotechadv.2014.05.006
18. Dutta K, Bochicchio D, Ribbe AE, et al. Symbiotic self-assembly strategy toward lipid-encased cross-linked polymer nanoparticles for efficient gene silencing. *ACS Appl Mater Interfaces*. 2019;11(28):24971–24983. doi:10.1021/acsami.9b04731
19. Wang H, Li F, Du C, et al. Doxorubicin and lapatinib combination nanomedicine for treating resistant breast cancer. *Mol Pharm*. 2014;11(8):2600–2611. doi:10.1021/mp400687w
20. Wang D, Xu X, Zhang K, et al. Codelivery of doxorubicin and MDR1-siRNA by mesoporous silica nanoparticles-polymerpolyethylenimine to improve oral squamous carcinoma treatment. *Int J Nanomedicine*. 2018;13:187–198. doi:10.2147/IJN.S150610
21. Wu Y, Zhang Y, Zhang W, et al. Reversing of multidrug resistance breast cancer by co-delivery of P-gp siRNA and doxorubicin via folic acid-modified core-shell nanomicelles. *Colloids Surf B Biointerfaces*. 2016;138:60–69. doi:10.1016/j.colsurfb.2015.11.041
22. Wang C, Guan W, Peng J, et al. Gene/paclitaxel co-delivering nanocarriers prepared by framework-induced self-assembly for the inhibition of highly drug-resistant tumors. *Acta Biomater*. 2020;103:247–258. doi:10.1016/j.actbio.2019.12.015
23. Forbes DC, Peppas NA. Polycationic nanoparticles for siRNA delivery: comparing ARGET ATRP and UV-initiated formulations. *ACS Nano*. 2014;8(3):2908–2917. doi:10.1021/nn500101c
24. Akinc A, Maier MA, Manoharan M, et al. The Onpattro story and the clinical translation of nanomedicines containing nucleic acid-based drugs. *Nat Nanotechnol*. 2019;14(12):1084–1087. doi:10.1038/s41565-019-0591-y
25. Prabha S, Vyas R, Gupta N, et al. RNA interference technology with emphasis on delivery vehicles-prospects and limitations. *Artif Cells Nanomed Biotechnol*. 2016;44(6):1391–1399. doi:10.3109/21691401.2015.1058808
26. Zhang J, Li X, Huang L. Non-viral nanocarriers for siRNA delivery in breast cancer. *J Control Release*. 2014;190:440–450. doi:10.1016/j.jconrel.2014.05.037
27. Lukashev AN, Zamyatnin AA Jr. Viral vectors for gene therapy: current state and clinical perspectives. *Biochemistry (Mosc)*. 2016;81(7):700–708. doi:10.1134/S0006297916070063
28. Wang Y, Luo Y-L, Chen Y-F, et al. Dually regulating the proliferation and the immune microenvironment of melanoma via nanoparticle-delivered siRNA targeting onco-immunologic CD155. *Biomater Sci*. 2020;8(23):6683–6694. doi:10.1039/d0bm01420f
29. Haggag YA, Ibrahim RR, Hafiz AA. Design, formulation and in vivo evaluation of novel honokiol-loaded PEGylated PLGA nanocapsules for treatment of breast cancer. *Int J Nanomedicine*. 2020;15:1625–1642. doi:10.2147/IJN.S241428
30. Haggag YA, Yasser M, Tambuwala MM, et al. Repurposing of Guanabenz acetate by encapsulation into long-circulating nanopolymersomes for treatment of triple-negative breast cancer. *Int J Pharmaceut*. 2021;600:120532. doi:10.1016/j.ijpharm.2021.120532
31. Haggag Y, Elshikh M, El-Tanani M, et al. Nanoencapsulation of sophorolipids in PEGylated poly(lactide-co-glycolide) as a novel approach to target colon carcinoma in the murine model. *Drug Deliv Transl Re*. 2020;10(5):1353–1366. doi:10.1007/s13346-020-00750-3
32. Kamerkar S, LeBleu VS, Sugimoto H, et al. Exosomes facilitate therapeutic targeting of oncogenic KRAS in pancreatic cancer. *Nature*. 2017;546(7659):498–503. doi:10.1038/nature22341
33. Wang MY, Zhang L, Cai Y, et al. Bioengineered human serum albumin fusion protein as target/enzyme/pH three-stage propulsive drug vehicle for tumor therapy. *Acs Nano*. 2020;14(12):17405–17418. doi:10.1021/acsnano.0c07610
34. Lee KJ, Ko EJ, Park Y-Y, et al. A novel nanoparticle-based theranostic agent targeting LRP-1 enhances the efficacy of neoadjuvant radiotherapy in colorectal cancer. *Biomaterials*. 2020;255:120151. doi:10.1016/j.biomaterials.2020.120151
35. Elzoghby AO, Samy WM, Elgindy NA. Albumin-based nanoparticles as potential controlled release drug delivery systems. *J Control Release*. 2012;157:168–182. doi:10.1016/j.jconrel.2011.07.031
36. Fang H, Gai Y, Wang S, et al. Biomimetic oxygen delivery nanoparticles for enhancing photodynamic therapy in triple-negative breast cancer. *J Nanobiotechnology*. 2021;19(1):81. doi:10.1186/s12951-021-00827-2
37. Chilom CG, Bălan A, Sandu N, et al. Exploring the conformation and thermal stability of human serum albumin corona of ferrihydrite nanoparticles. *Int J Mol Sci*. 2020;21(24):9734. doi:10.3390/ijms21249734
38. Zhou Y, Ren X, Hou Z, et al. Engineering a photosensitizer nanoplatform for amplified photodynamic immunotherapy via tumor microenvironment modulation. *Nanoscale Horiz*. 2021;6(2):120–131. doi:10.1039/d0nh00480d
39. Sleep D. Albumin and its application in drug delivery. *Expert Opin Drug Del*. 2015;12(5):793–812. doi:10.1517/17425247.2015.993313
40. Low K, Wacker M, Wagner S, Langer K, von Briesen H. Targeted human serum albumin nanoparticles for specific uptake in EGFR-expressing colon carcinoma cells. *Nanomedicine*. 2011;7(4):454–463. doi:10.1016/j.nano.2010.12.003
41. Zhang X, Li Y, Wei M, et al. Cetuximab-modified silica nanoparticle loaded with ICG for tumor-targeted combinational therapy of breast cancer. *Drug Deliv*. 2019;26(1):129–136. doi:10.1080/10717544.2018.1564403
42. Hofmann M, McCormack E, Mujic M, et al. Increased plasma colloid osmotic pressure facilitates the uptake of therapeutic macromolecules in a xenograft tumor model. *Neoplasia*. 2009;11:812–822. doi:10.1593/neo.09662
43. Gudino V, Pohl SÖ-G, Billard CV, et al. RAC1B modulates intestinal tumourigenesis via modulation of WNT and EGFR signalling pathways. *Nat Commun*. 2021;12:2335. doi:10.1038/s41467-021-22531-3
44. Lu ZY, Truex NL, Melo MB, et al. IgG-engineered protective antigen for cytosolic delivery of proteins into cancer cells. *Acs Central Sci*. 2021;7:365–378. doi:10.1021/acscentsci.0c01670
45. Sharifpour E, Ghaedi M, Asfaram A, et al. Modeling and optimization of ultrasound-assisted high performance adsorption of basic Fuchsin by starch-capped zinc selenide nanoparticles/AC as a novel composite using response surface methodology. *Int J Biol Macromol*. 2020;152:913–921. doi:10.1016/j.ijbiomac.2020.02.236
46. Foster DJ, Brown CR, Shaikh S, et al. Advanced siRNA designs further improve in vivo performance of GalNAc-siRNA conjugates. *Mol Ther*. 2018;26(3):708–717. doi:10.1016/j.ymthe.2017.12.021
47. Han NN, Li X, Tao L, Zhou Q. Doxorubicin and rhein loaded nanomicelles attenuates multidrug resistance in human ovarian cancer. *Biochem Biophys Res Commun*. 2018;498(1):178–185. doi:10.1016/j.bbrc.2018.01.042
48. Yu J, Zhou P, Asenso J, et al. Advances in plant-based inhibitors of P-glycoprotein. *J Enzyme Inhib Med Chem*. 2016;31:867–881. doi:10.3109/14756366.2016.1149476
49. Lusvarghi S, Ambudkar SV. ATP-dependent thermostabilization of human P-glycoprotein (ABCB1) is blocked by modulators. *Biochem J*. 2019;476(24):3737–3750. doi:10.1042/Bcj20190736
50. Zhang YJ, Sun T, Jiang C. Biomacromolecules as carriers in drug delivery and tissue engineering. *Acta Pharmaceutica Sinica B*. 2018;8(1):34–50. doi:10.1016/j.apsb.2017.11.005
51. Ryu JH, Shin J-Y, Kim SA, et al. Non-invasive optical imaging of matrix metalloproteinase activity with albumin-based fluorogenic nanoprobes during angiogenesis in a mouse hindlimb ischemia model. *Biomaterials*. 2013;34(28):6871–6881. doi:10.1016/j.biomaterials.2013.05.074